Supercontinuum generation at 800 nm in all-normal dispersion photonic crystal fiber

Igor A. Sukhoivanov,[1] Sergii O. Iakushev,[2] Oleksiy V. Shulika,[1,*] José Amparo AndradeLucio,[1] Antonio Díez,[3] and Miguel Andrés[3]

[1]*Universidad de Guanajuato, DICIS, Salamanca, GTO, Mexico*
[2] *Kharkov National University of Radio Electronics, Kharkov, Ukraine*
[3]*Universidad de Valencia, Burjassot (Valencia), Spain*
[*]*oshulika@ugto.mx*

Abstract: We have numerically investigated the supercontinuum generation and pulse compression in a specially designed all-normal dispersion photonic crystal fiber with a flat-top dispersion curve, pumped by typical pulses from state of the art Ti:Sapphire lasers at 800 nm. The optimal combination of pump pulse parameters for a given fiber was found, which provides a wide octave-spanning spectrum with superb spectral flatness (a drop in spectral intensity of ~1.7 dB). With regard to the pulse compression for these spectra, multiple-cycle pulses (~8 fs) can be obtained with the use of a simple quadratic compressor and nearly single-cycle pulses (3.3 fs) can be obtained with the application of full phase compensation. The impact of pump pulse wavelength-shifting relative to the top of the dispersion curve on the generated SC and pulse compression was also investigated. The optimal pump pulse wavelength range was found to be $750\ \text{nm} < \lambda_p < 850\ \text{nm}$, where the distortions of pulse shape are quite small (< -3.3 dB). The influences of realistic fiber fabrication errors on the SC generation and pulse compression were investigated systematically. We propose that the spectral shape distortions generated by fiber fabrication errors can be significantly attenuated by properly manipulating the pump.

OCIS codes: (190.4370) Nonlinear optics, fibers; (320.7110) Ultrafast nonlinear optics; (320.6629) Supercontinuum generation; (060.5295) Photonic crystal fibers.

References and links

1. J. M. Dudley, J. R. Taylor *Supercontinuum Generation in Optical Fibers*, (Cambridge, 2010).
2. R. R. Alfano, *The Supercontinuum Laser Source*, 2nd ed. (Springer, 2006).
3. J. M. Dudley, G. Genty, and S. Coen, "Supercontinuum generation in photonic crystal fiber," Rev. Mod. Phys. **78**(4), 1135–1184 (2006).
4. J. Herrmann, U. Griebner, N. Zhavoronkov, A. Husakou, D. Nickel, J. Knight, W. Wadsworth, P. S. J. Russell, and G. Korn, "Experimental evidence for supercontinuum generation by fission of higher-order solitons in photonic crystal fibers," Phys. Rev. Lett. **88**(17), 173901 (2002).
5. X. Gu, L. Xu, M. Kimmel, E. Zeek, P. O'Shea, A. P. Shreenath, R. Trebino, and R. S. Windeler, "Frequency-resolved optical gating and single-shot spectral measurements reveal fine structure in microstructure-fiber continuum," Opt. Lett. **27**(13), 1174–1176 (2002).
6. K. L. Corwin, N. R. Newbury, J. M. Dudley, S. Coen, S. A. Diddams, K. Weber, and R. S. Windeler, "Fundamental noise limitations to supercontinuum generation in microstructure fiber," Phys. Rev. Lett. **90**(11), 113904 (2003).
7. N. R. Newbury, B. R. Washburn, and K. L. Corwin, "Noise amplification during supercontinuum generation in microstructure fiber," Opt. Lett. **28**(11), 944–946 (2003).
8. K. M. Hilligsøe, T. Andersen, H. Paulsen, C. Nielsen, K. Mølmer, S. Keiding, R. Kristiansen, K. Hansen, and J. Larsen, "Supercontinuum generation in a photonic crystal fiber with two zero dispersion wavelengths," Opt. Express **12**(6), 1045–1054 (2004).

#224230 - $15.00 USD Received 1 Oct 2014; revised 5 Nov 2014; accepted 11 Nov 2014; published 26 Nov 2014

9. M. Frosz, P. Falk, and O. Bang, "The role of the second zero-dispersion wavelength in generation of supercontinua and bright-bright soliton-pairs across the zero-dispersion wavelength," Opt. Express **13**(16), 6181–6192 (2005).
10. M.-L. V. Tse, P. Horak, F. Poletti, N. G. Broderick, J. H. Price, J. R. Hayes, and D. J. Richardson, "Supercontinuum generation at 1.06 μm in holey fibers with dispersion flattened profiles," Opt. Express **14**(10), 4445–4451 (2006).
11. K. R. Tamura, H. Kubota, and M. Nakazawa, "Fundamentals of Stable Continuum Generation at High Repetition Rates," IEEE J. Quant. Electron., **36**(7), 773-779 (2000).
12. Y. Takushima, F. Futami, and K. Kikuchi, "Generation of over 140-nm-wide Super-Continuum from a Normal Dispersion Fiber by using a Mode-Locked Semiconductor Laser Source," IEEE Photon. Technol. Let., **10(**11**),** 1560-1562 (1998).
13. K. Mori, H. Takara, S. Kawanishi, M. Saruwatari and T. Morioka, "Flatly broadened supercontinuum spectrum generated in a dispersion decreasing fibre with convex dispersion profile," Electron. Let., **33**(21), 1806-1808 (1997).
14. H. Sotobayashi and K. Kitayama, "325nm bandwidth supercontinuum generation at 10Gbit/s using dispersion flattened and non-decreasing normal dispersion fibre with pulse compression," Electron. Let., **34**(13), 1336-1337 (1998).
15. G. A. Nowak, J. Kim, and M. N. Islam, "Stable supercontinuum generation in short lengths of conventional dispersion-shifted fiber," App. Opt., **38**(36), 7364-7369 (1999).
16. A. M. Heidt, A. Hartung, G. W. Bosman, P. Krok, E. G. Rohwer, H. Schwoerer, and H. Bartelt, "Coherent octave spanning near-infrared and visible supercontinuum generation in all-normal dispersion photonic crystal fibers," Opt. Express **19**(4), 3775–3787 (2011).
17. L. E. Hooper, P. J. Mosley, A. C. Muir, W. J. Wadsworth, and J. C. Knight, "Coherent supercontinuum generation in photonic crystal fiber with all-normal group velocity dispersion," Opt. Express **19**(6), 4902–4907 (2011).
18. A. M. Heidt, "Pulse preserving flat-top supercontinuum generation in all-normal dispersion photonic crystal fibers," J. Opt. Soc. Am. B **27**(3), 550–559 (2010).
19. *Nonlinear Photonic Crystal Fiber NL-1050-NEG-1*, http://www.nktphotonics.com
20. G Stepniewski, M Klimczak, H Bookey, B Siwicki, D Pysz, R Stepien, A K Kar, A J Waddie, M R Taghizadeh and R Buczynski, "Broadband supercontinuum generation in normal dispersion all-solid photonic crystal fiber pumped near 1300 nm", Laser Phys. Lett. **11**(5), 055103, (2014).
21. N. Nishizawa and J. Takayanagi, "Octave spanning high-quality supercontinuum generation in all-fiber system," J. Opt. Soc. Am. B **24**(8), 1786–1792 (2007).
22. G. P. Agrawal, *Nonlinear Fiber Optics*, 4th ed. (Academic Press, 2007).
23. K. J. Blow and D. Wood, "Theoretical Description of Transient Stimulated Scattering in Optical Fibers", IEEE J. Quantum Electron. **25**(12), 2665-2673 (1989).
24. J. Hult, "A fourth-order runge–kutta in the interaction picture method for simulating supercontinuum generation in optical fibers," J. Lightwave Technol. **25(**12), 3770 –3775 (2007).
25. M. Koshiba and K. Saitoh, "Applicability of classical optical fiber theories to holey fibers," Opt. Lett. **29**(15), 1739–1741 (2004).
26. K. Saitoh and M. Koshiba, "Empirical relations for simple design of photonic crystal fibers," Opt. Express **13**(1), 267–274 (2005).
27. A. M. Heidt, J. Rothhardt, A. Hartung, H. Bartelt, E. G. Rohwer, J. Limpert, and A. Tünnermann, "High quality sub-two cycle pulses from compression of supercontinuum generated in all-normal dispersion photonic crystal fiber," Opt. Express **19**(15), 13873-13879 (2011).
28. S. Demmler, J. Rothhardt, A. M. Heidt, A. Hartung, E. G. Rohwer, H. Bartelt, J. Limpert, and A. Tünnermann, "Generation of high quality, 1.3 cycle pulses by active phase control of an octave spanning supercontinuum," Opt. Express **19**(21), 20151-20158 (2011).
29. F. X. Kärtner, *Few-Cycle Laser Pulse Generation and its Applications* (Springer, 2004).
30. Y. Liu, H. Tu, and S. A. Boppart, "Wave-breaking-extended fiber supercontinuum generation for high compression ratio transform-limited pulse compression," Opt. Lett. **37**(12), 2172-2174 (2012).
31. David Castelló-Lurbe, Pedro Andrés, and Enrique Silvestre, "Dispersion-to-spectrum mapping in nonlinear fibers based on optical wave-breaking," Opt. Express. **21**(23), 28550-28558 (2013).
32. B. Schenkel, J. Biegert, U. Keller, C. Vozzi, M. Nisoli, G. Sansone, S. Stagira, S. De Silvestri, and O. Svelto, "Generation of 3.8-fs pulses from adaptive compression of a cascaded hollow fiber supercontinuum," Opt. Lett. **28**(20), 1987-1989 (2003).

1. Introduction

Supercontinuum (SC) generation has become a very active field of research during the last decade. Significant interest in this field was inspired by the application of specially designed photonic crystal fibers (PCFs) and tapered fibers, which have allowed SC generation in a much wider range of source parameters than that possible with bulk media or conventional fibers [1]. Due to its unique properties, the SC has found numerous applications in optical

#224230 - $15.00 USD Received 1 Oct 2014; revised 5 Nov 2014; accepted 11 Nov 2014; published 26 Nov 2014

communications, optical coherence tomography, frequency metrology, and extremely short pulse generation [2]. The key features of novel fibers that are important for producing SC are a high nonlinear coefficient, in addition to flexibility in tailoring the dispersion profile. The first factor is important for producing an SC even with low-energy pulses (a few nanojoules). With regard to the second factor, the relationship between the input pump wavelength and the dispersion profile of the fiber directly governs the properties of the generated SC. It was found that the broadest SC spectra are generated when the pump pulse is injected into the anomalous group velocity dispersion (GVD) region near the zero-dispersion wavelength (ZDW) of the fiber [3]. In this case, SC generation appears in the anomalous dispersion region of the optical fibers. Correspondingly, the broadening mechanism here is dominated by soliton dynamics and soliton fission, which are sensitive to the input pulse fluctuations and the pump laser shot noise [4]. This broadening mechanism leads to several problems, such as a complex temporal profile, lack of spectral flatness, increase of noise, and low coherence characteristics [5–7]. In response to these problems, fibers with two closely spaced ZDWs were proposed for achieving SC generation [8]. This resulted in a stable and coherent SC spectrum generation with two distinct spectral peaks on the normal dispersion side of each ZDW [8–10], which is undesirable if a continuous broadband spectrum is required.

The generation of supercontinuum spectra in normal dispersion fibers has been investigated previously in 1990s using single mode fibers with dispersion-flattened normal dispersion and a few picosecond pump pulses [11-14] and subpicosecond ones [15]. This allowed achieving flat and coherent SC spectra in the wavelength range up to 325 nm (0.3 octave) [4]. Recently it was shown that highly nonlinear all-normal dispersion photonic crystal fibers (ANDi PCFs), which exhibit convex dispersion profiles lying completely in the normal dispersion region, can be successfully fabricated. Pumping by femtosecond few-nJ pulses near the flattened top of the dispersion curves for such ANDi PCFs generates highly coherent, flat-top, octave-spanning SCs, thereby preserving a single pulse in temporal the domain [16, 17]. The physical mechanism of SC generation in ANDi PCFs differs dramatically from the corresponding mechanism in the anomalous region of the fibers. In the normal dispersion region, spectral broadening appears due to the action of self-phase modulation (SPM) and four-wave mixing (FWM) induced by optical wave breaking (OWB) [16, 18]. It was shown that pumping near the flat top of the dispersion curve is essential for providing maximal spectral broadening and spectral flatness [18], whereas pumping far away from the flat top leads to the degradation of the spectral flatness [16]. Until now, there have only been a few proposed designs for an ANDi PCF with a flat-top dispersion curve located at near-infrared wavelength (e.g., 1060 nm [17, 19], 1300 nm [20], 1690 nm [21]), and in the visible range (e.g., 650 nm [16]). However, the wavelength of 800 nm is important from a practical point of view, because this is precisely where Ti:Sapphire lasers and Erbium-doped fiber lasers with second harmonic generation emit. It was shown that for pumping at 800 nm one can use an ANDi PCF with a flat top at 650 nm [16]. However, such a fiber is not optimal for pumping with 800 nm, and has extremely small geometrical parameters (a pitch of 0.67 μm, and a relative hole diameter of 0.6).

In response to the demand for such a device, we have designed an ANDi PCF with a flat-top dispersion curve with maximum dispersion coefficient D located at 800 nm, and with larger pitch than previously achieved. Furthermore, we investigate this device's applicability for SC generation with femtosecond pulses delivered by conventional Ti:Sapphire lasers. We also investigate the impact of pump pulse parameters, such as pump pulse energy and pulse duration, on the generated SC. The optimal combination of pump pulse parameters for a given fiber is found, which yields both maximum spectral width and perfect spectral flatness. As regards pulse compression for these SC spectra, a quadratic compressor can yield multiple-cycle pulses, while the application of full phase compensation can yield single-cycles pulses. We also investigate the impact of pump pulse wavelength shifting with respect to the top of the dispersion curve on the generated SC and pulse compression. Special attention is paid to

#224230 - $15.00 USD Received 1 Oct 2014; revised 5 Nov 2014; accepted 11 Nov 2014; published 26 Nov 2014

the influence of realistic fiber fabrication errors on the SC generation in ANDi PCFs, which could produce the distortions of the spectral shape of the generated SC. Lastly, an approach for the correction of the spectral shape distortions is proposed based on a proper variation of the pump pulse parameters, and depending on the nature of the fabrication error.

2. Theory

SC generation in optical fibers is well described by the generalized nonlinear Schrödinger equation (GNLSE) [1, 3, 22]. Here we apply the GNLSE for the electric field envelope $A(z,T)$ at a propagation distance z in a retarded reference time frame $T = t - \beta_1 z$ in the following form:

$$\frac{\partial A(z,T)}{\partial z} = (\hat{D} + \hat{N})A(z,T), \tag{1}$$

where $\hat{D}$ is a linear operator, and $\hat{N}$ is a nonlinear operator. The linear operator $\hat{D}$ can be written in the following form [1, 3]:

$$\hat{D} = -\frac{\alpha}{2} + \left(\sum_{k\geq 2} \frac{i^{k+1}}{k!} \beta_k \frac{\partial^k}{\partial T^k} \right). \tag{2}$$

The first term the operator $\hat{D}$ gives the linear loss in the fiber α, whereas the second one describes dispersion, where β_k are the dispersion coefficients associated with the Taylor series expansion of the propagation constant $\beta(\omega)$ about the central frequency of the pump pulse spectrum, ω_0. However, in this paper the dispersion operator is calculated in the frequency domain by multiplying the complex spectral envelope $\tilde{A}(z,\omega)$ with the operator $\left(\beta(\omega) - \omega\beta_1 - \beta_0\right)$. In this case, the dispersion is given directly by the propagation constant $\beta(\omega)$, computed from the geometrical parameters of the fiber, along with the dispersion coefficients β_0 and β_1.

The nonlinear operator $\hat{N}$ in Eq. (1) is written in the following way:

$$\hat{N} = i\gamma \frac{1}{A(z,T)} \left(1 + i\tau_{\text{shock}} \frac{\partial}{\partial T}\right) \times \left(A(z,T) \int_{-\infty}^{\infty} R(T') \left| A(z, T - T') \right| dT' \right). \tag{3}$$

Eq. (3) includes SPM associated with a nonlinear coefficient γ. The time derivative in the nonlinear operator $\hat{N}$ includes the effects of self-steepening and optical shock formation, characterized on a time scale $\tau_{\text{shock}} = 1/\omega_0$. The response function $R(t) = (1 - f_R)\delta(t) + f_R h_R(t)$ includes both the instantaneous electronic contributions, as well as the delayed Raman contributions, with $f_R = 0.18$ representing the fractional contribution of the delayed Raman response. For the Raman response function of the silica fiber, $h_R(t)$, the analytical expression used is [23]:

$$h_R(t) = \frac{\tau_1^2 + \tau_2^2}{\tau_1 \tau_2^2} \exp\left(-\frac{t}{\tau_2}\right) \sin\left(\frac{t}{\tau_1}\right), \tag{4}$$

where the parameters $\tau_1 = 12.2$ fs and $\tau_2 = 32$ fs are adjustable and chosen to provide a good fit to the actual Raman-gain spectrum [23]. The inverse time scale $1/\tau_1$ gives the phonon frequency, and $1/\tau_2$ determines the bandwidth of the Lorentzian line. The nonlinear coefficient γ is defined as follows:

#224230 - $15.00 USD Received 1 Oct 2014; revised 5 Nov 2014; accepted 11 Nov 2014; published 26 Nov 2014

$$\gamma = \frac{\omega_0 n_2(\omega_0)}{c A_{\text{eff}}(\omega_0)}, \tag{5}$$

where $n_2 = 2.9\times10^{-20}\ \text{m}^2/\text{W}$ is the nonlinear refractive index of the silica glass, c is the vacuum speed of light, and A_{eff} is the effective mode field area of the fiber. Eq. (1), the GNLSE, is solved numerically by means of the method proposed in [1], which proceeds by finding the solution in the frequency domain while making use of a change of variables to shift into the so-called interaction picture [24].

3. Fiber Design

We have designed an ANDi PCF suitable for SC generation at 800 nm; its characteristics are shown in Fig. 1. The dispersion profile and mode field diameter (MFD) of the PCF were calculated with the analytical method described in [25, 26]. The designed ANDi PCF has a fused-silica solid core and a hexagonal lattice of air holes in the cladding region, with a pitch of Λ = 1.0 μm and a relative hole size of $d/\Lambda = 0.5$. Dispersion and nonlinear coefficients of this fiber at 800 nm are as follows: $D = -40\ \text{ps/(nm}\cdot\text{km)}$, and $\gamma = 1131/(\text{W}\cdot\text{km})$. However, one has to note that the design parameters of the fiber can vary due to various experimental factors during the drawing process. Figure 2 shows the cross-section and the core of the designed ANDi-PCF sample, which shows that Λ = 1.0 μm and d = 0.53 μm. The fiber was fabricated according to the stack-and-draw procedure. Silica capillaries were stacked together to form hexagonal preforms with seven rings of air holes arranged around a solid silica core. Special attention was paid to the drawing parameters during the fabrication in order to prevent the collapse of the holes. Although the hole's diameter is somewhat larger than the nominal value, we do not expect significant variations of the dispersion curve. Therefore, calculated data for the ideal structure are used for the first SC simulations.

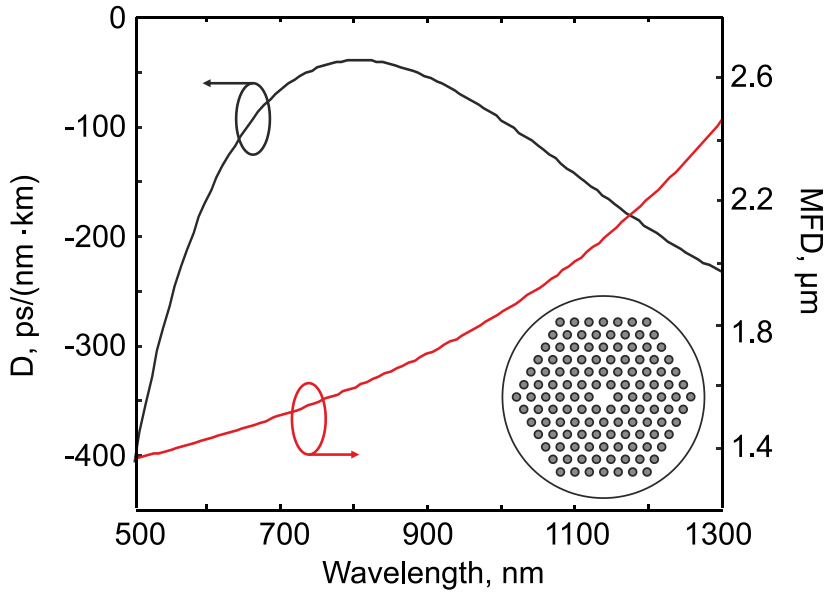

Fig. 1. Calculated dispersion profile and mode field diameter (MFD) of an all normal dispersion photonic crystal fiber (ANDi PCF).

#224230 - $15.00 USD Received 1 Oct 2014; revised 5 Nov 2014; accepted 11 Nov 2014; published 26 Nov 2014

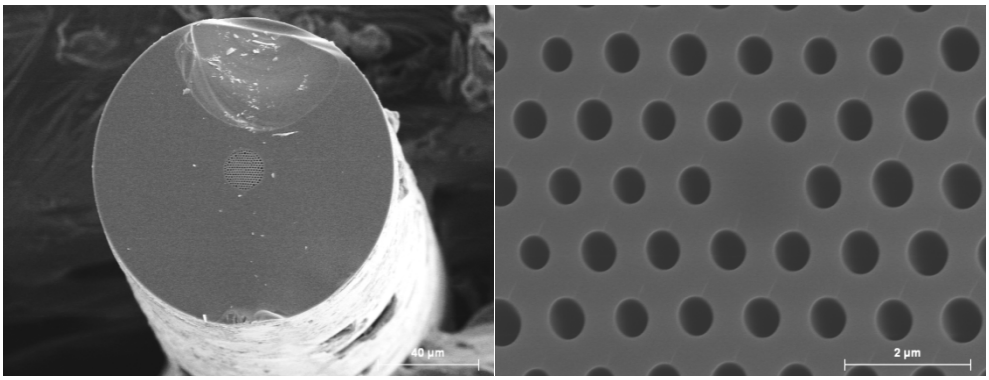

Fig. 2. Microphotography of the cross-section and the core of the fabricated all-normal dispersion photonic crystal fiber (ANDi PCF), with Λ= 1.0 µm and d = 0.53 µm.

4. Variation of pump pulse energy and duration

First we investigate SC generation in the designed ANDi PCF. For pumping, we take initial, unchirped Gaussian pulses similar to those produced by conventional Ti:Sapphire lasers with a pulse duration (FWHM) of 50-150 fs and a pulse energy of 5-10 nJ (repetition rate 80 MHz). Fig. 3 shows the simulation results of SC generation in the designed ANDi PCF using a 10 cm piece of fiber. Fig. 3(a) shows output pulses in the temporal domain for different initial pulse energies and durations. One can see that in the temporal domain a single pulse is preserved. However, the pulse shape is not Gaussian and pulse duration increases up to a few picoseconds. Fig. 3(b) shows the corresponding spectra of those pulses. For a fixed peak power (e.g., 47 kW) of the initial pulse (i.e., in the cases of 2.5 nJ, 50 fs; 5 nJ, 100 fs; and 7.5 nJ, 150 fs) the spectral width is nearly the same for all cases (~580 nm) corresponding to ~1.0 octave. Generated spectra have perfect flatness in the aforementioned cases, as Fig. 3(c) shows. The drop in spectral intensity at the central part of each spectrum is about 1.7 dB.

In order to increase the spectral width, one has to increase the peak power of the pump pulse. If we increase the initial pulse energy (10 nJ, 100 fs) or reduce the pulse width (5 nJ, 50 fs) such that the peak power is 94 kW, then spectral width is increased up to ~720 nm, corresponding to ~1.3 octave. However, the price for that increased spectral width is a worsening of spectral flatness. Fig. 3(c) shows that in these cases, the drop in spectral intensity at the central part of each spectrum is about 3.5 dB. Additional spectral broadening is accompanied by the depletion of the central part of the spectrum, such that a dip appears at the pumping wavelength. Furthermore, spectral splitting appears as a result of the complex dynamics of spectral broadening in the ANDi PCF. This is due to nonlinear effects of self-steepening and the frequency dependence of the nonlinear coefficient, in combination with the SPM and an optical-wave-breaking-induced FWM process, which are considered in details in [18]. Thus, one has to find some compromise between impressive spectral flatness and maximal spectral width by varying the initial pump pulse. For the given fiber, we can see that the peak power of the pump pulse at 47 kW provides quite large spectral bandwidth up to 1 octave, and perfect spectral flatness at the same time. From the results of this simulation, we conclude that the most suitable pump is 47 kW of peak power characterized by a pulse with energy of 5 nJ and a duration of 100 fs. This pairing of pulse energy and duration is easily achievable with the majority of modern femtosecond lasers.

#224230 - $15.00 USD Received 1 Oct 2014; revised 5 Nov 2014; accepted 11 Nov 2014; published 26 Nov 2014

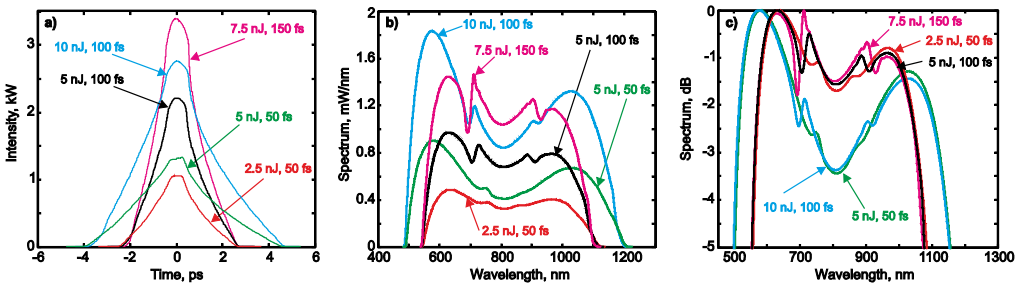

Fig. 3. Supercontinuum generation in an all-normal dispersion photonic crystal fiber (ANDi PCF) of 10 cm length at 800 nm. a) Pulse profiles in temporal domain. b) Pulse spectra. c) Pulse spectra in a logarithmic scale. Peak powers of pump pulses are (color coded) 44 kW, 88 kW, 44 kW, 88 kW, 44 kW.

Because of single-pulse preservation with a smooth temporal profile, SC generation in ANDi PCFs is attractive for subsequent pulse compression. Compression of pulses up to 26 fs [17], 5.0 fs [27], and 3.64 fs [28] with SC spectra generated in ANDi PCFs was previously reported. The most attractive aspect is the possibility to generate multiple-cycle pulses, since such pulses are highly important in time-resolved studies of fundamental processes in physics, chemistry and biology [29]. Previous studies [27, 28] used commercially available fibers with a flat top located at 1060 nm [19], as well as special oscillators that produce very short pulses for the fiber's pump (15 fs in [27] and 6 fs in [28]). Here we examine the applicability of specially designed ANDi PCFs with a flat top at 800 nm, in combination with conventional Ti:Sapphire lasers for short pulse generation. The chirp of pulses produced at the output of ANDi PCFs is already quite close to being linear [18]. Therefore, one can expect that a simple compression technique should yield impressive compression results. First we investigate the application of a simple quadratic compressor for the compensation of a linear chirp. This can be achieved, for example, by gratings or prism pairs. Fig. 4(a) shows simulation results of pulse compression for pulses obtained at the output of the ANDi PCF shown in Fig. 3(a). The amount of group delay dispersion of the compressor in each case was chosen in order to obtain the highest peak power of the compressed pulse. This usually corresponds to the shortest pulse duration as well.

From Fig. 4(a) we can see at first that pump pulses with an increased peak power of 94 kW (10 nJ, 100 fs; 5 nJ, 50 fs) and wider SC spectra do not provide better compression results if a simple quadratic compression is used. The best result for the 47 kW pump (7.5 nJ, 150 fs) is achieved by providing a compressed pulse with a duration of 7.6 fs and a peak power of ~330 kW. We assume that this is due to the larger pump pulse duration of 150 fs, which induces a smaller nonlinear chirp during SC generation. In other cases, the impact of uncompensated nonlinear chirp is larger, and therefore compression results are worse due to the stronger impact of nonlinear effects when the initial pulse duration is shorter. The visible results of non-ideal compression are excessive oscillated pulse tails in all cases in Fig. 4(a). Nevertheless, the pump combination (5 nJ, 100 fs) provides a nicely compressed pulse with a peak power of ~200 kW and a duration of 8.1 fs, which corresponds to ~3 cycles of optical field of the pulse at 800 nm.

If a quadratic compressor is used, the nonlinear chirp remains uncompressed. However, more sophisticated compression techniques can be also applied, which are able to compensate for nonlinear chirp [28, 30, 32], providing shorter pulses up to the transform-limited one. Therefore, we also investigate the case of full phase compensation. Fig. 4(b) shows simulation results of pulse compression for pulses obtained at the output of ANDi PCFs when full phase compensation is applied. We can see that the potential of wider spectral bandwidth is fully exploited and shorter pulses are obtained from initial pulses with an increased peak power of 94 kW (10 nJ, 100 fs; 5 nJ, 50 fs). In these cases, pulse duration is as short as 2.5 fs, which corresponds to one cycle of the optical field at 800 nm. Application of 47 kW peak power (2.5

#224230 - $15.00 USD Received 1 Oct 2014; revised 5 Nov 2014; accepted 11 Nov 2014; published 26 Nov 2014

nJ, 50 fs; 5 nJ, 100 fs; 7.5 nJ, 150 fs) provides compressed pulses with 3.3 fs, whereas peak power is varied depending on the energy of the pump pulse.

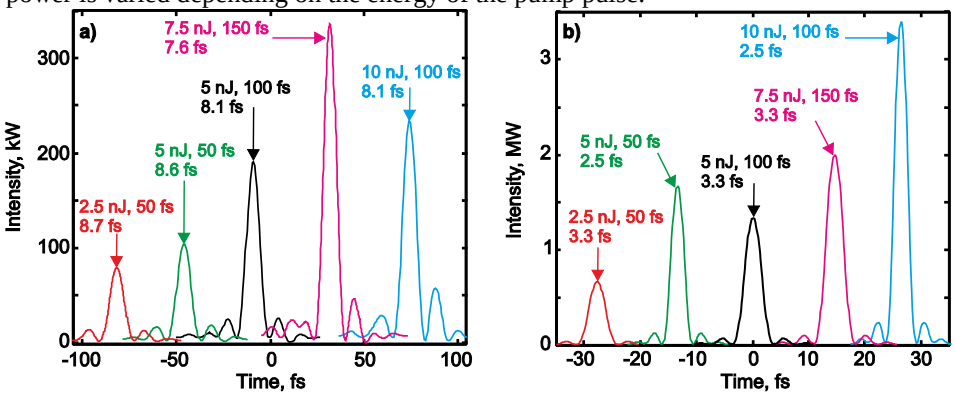

Fig. 4. Compression of pulses obtained at the output of the all-normal dispersion photonic crystal fiber (ANDi PCF) shown in Fig. 3 a). a) Compensation of only linear chirp. b) Full phase compensation. Peak powers of pump pulses are (color coded) 44 kW, 88 kW, 44 kW, 88 kW, 44 kW.

Thus, application of specially designed ANDi PCFs with a flat top at 800 nm, together with a conventional Ti:Sapphire laser, allows multiple-cycle pulses to be obtained (if a simple quadratic compressor is used) and single-cycle pulses to be obtained (if full phase compensation is applied).

5. Shifting the wavelength of pump pulse

Another important issue concerns the spectral changes that appear when the pump wavelength is shifted from the top of the dispersion curve of the ANDi PCF (800 nm in our case). The tuning range of typical Ti:Sapphire lasers is 700-900 nm. Therefore we investigated what happens if pumping is adjusted within this tuning range. Fig. 5 shows results of SC generation and pulse compression at different pump wavelengths for the optimal combination of pump parameters (5 nJ, 100 fs) stated in the previous section.

First we note that shifting of pump wavelength leads to a steepening of the pulse edges, as Fig. 5(a) shows. Redshifting (850 nm, 900 nm) leads to the steepening of the trailing edge, whereas blueshifting (750 nm, 700 nm) leads to the steepening of the leading edge of the pulse. However, the most essential changes appear in the spectral domain. From Fig. 5(b) one can see that the shifting of the pump wavelength leads to a strong asymmetry of the spectrum, and shifts the spectrum itself as well. At 700 nm, the blue part of the spectrum is amplified, whereas the red spectral part is depleted, and the spectrum is shifted towards the shorter wavelengths. The drop in spectral intensity in the central part of the spectrum is 5 dB in this case. At 750 nm the spectral asymmetry is weaker, with a drop of only 3.3 dB. The opposite picture appears at 900 nm, where the red part of the spectrum is amplified as compared to the blue spectral part. The drop of spectral intensity in the central part of the spectrum is 3.9 dB at 900 nm and 2.4 dB at 850 nm. Thus, we suppose that the optimal pump wavelength range for obtaining SC spectra with sufficient flatness in the designed ANDi PCF is within the range $750\,\text{nm} < \lambda_p < 850\,\text{nm}$. One has to note that similar spectral distortions were observed experimentally when the pumping wavelength was shifted to a shorter wavelength of ~200 nm as compared to the top of dispersion curve [16]. Here we can see that spectral asymmetry appears when the pump wavelength shifts to either side of the top of the dispersion curve, following the dispersion-to-spectrum mapping rules derived for a system where SPM is the most relevant nonlinear effect [31]. Moreover, the strong spectral asymmetry appears more readily for $\pm 100\,\text{nm}$ shift. This is related to the stronger curvature of the dispersion curve of

#224230 - $15.00 USD Received 1 Oct 2014; revised 5 Nov 2014; accepted 11 Nov 2014; published 26 Nov 2014

the designed ANDi PCF at 800 nm, whereas the fiber *NL-1050-NEG-1* [19] used in [16] has a wider flattened top at 1060 nm.

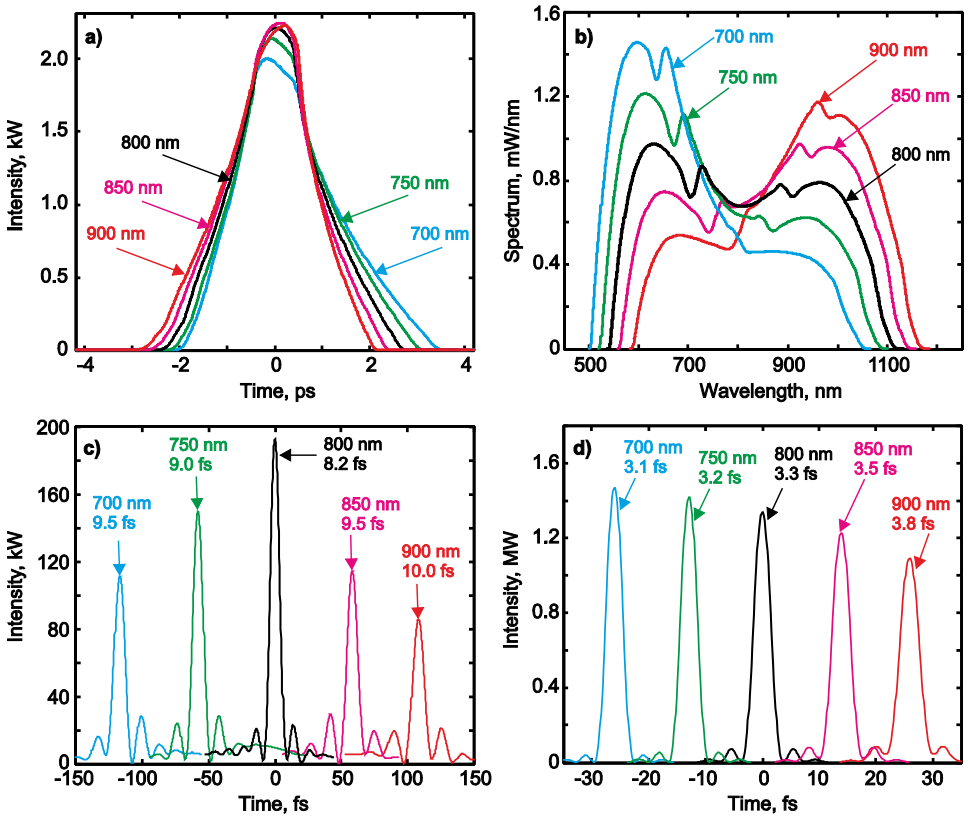

Fig. 5. Supercontinuum generation and pulse compression in an all-normal dispersion photonic crystal fiber (ANDi PCF) of 10 cm length at different wavelengths. In all cases, the initial pulse energy is 5 nJ and the pulse duration is 100 fs, which corresponds to 44 kW of peak power. a) Pulse profiles in temporal domain. b) Pulse spectra. c) Compressed pulses with compensation of only a linear chirp. d) Compressed pulses, full phase compensation.

It is natural to expect that such changes of pulse wave forms and its spectral shape due to the shifting of pump pulse wavelength will influence the pulse compression as well. From Fig. 5(c) we see that the shifting of pulse wavelength leads to worse compression results throughout if a quadratic compressor is used; pulse durations are larger for all cases and peak powers are lower as compared to the pump at 800 nm. If full phase compensation is applied (Fig. 5(d)) we can see that for redshifting compression results are also worse than those for the pump at 800 nm. However, for blueshifting we obtain moderately improved compression results. We suppose that this is related to the blueshifting of the spectra, such that spectral content of the frequency spectrum becomes slightly wider at shorter wavelengths. Thus, within the wavelength range $750\,\text{nm} < \lambda_p < 850\,\text{nm}$ we can obtain a compressed pulse duration of 9.5-8.2 fs if a quadratic compressor is used, and 3.5-3.2 fs if full phase compensation is applied.

6. Impact of fabrication errors

During the fabrication of microstructured optical fibers, various errors can appear leading to the deviation of the fiber's geometrical parameters – such as pitch, hole diameter, and hole shape – from the designed ones. Thus, it is important to estimate the influence of fabrication

#224230 - $15.00 USD Received 1 Oct 2014; revised 5 Nov 2014; accepted 11 Nov 2014; published 26 Nov 2014

errors on the fiber properties and subsequent SC generation in the fiber. During the fabrication of microstructured optical fiber by the stack-and-draw process, independent variation among pitch and hole diameter can be up to 5-10%. Here we investigate the influence of hole-diameter deviation and pitch deviation from the designed values (Λ = 1.0 μm, d = 0.5 μm on the properties of ANDi PCFs and the SC generation. All simulations in this section were made for the optimal combination of pump parameters (i.e., 5 nJ, 100 fs, corresponding to 44 kW of peak power) at 800 nm.

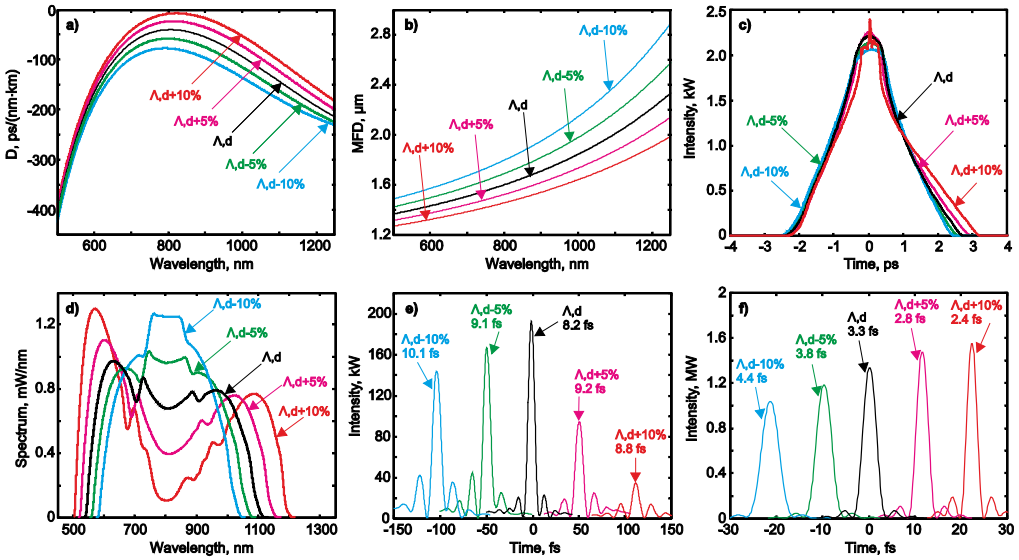

Fig. 6. The influence of fabrication errors on the properties of an all-normal dispersion photonic crystal fiber (ANDi PCF), supercontinuum (SC) spectrum, and pulse compression. Only diameter of air holes is changed ($\Lambda, d \pm 5\%; \Lambda, d \pm 10\%$). a) Fiber's dispersion. b) Mode field diameter (MFD), c) Pulse profiles in temporal domain. d) Pulse spectra. e) Compressed pulses with compensation of only a linear chirp. f) Compressed pulses, full phase compensation.

Fig. 6(a) shows dispersion curves of an ANDi PCF when only the diameter of air holes is changed. One can see that the main features in this case are the rise of the dispersion curve and the slight shift to longer wavelengths when d is increased. For this deviation ($\Lambda, d + 10\%$) the top of dispersion curve is already close to the zero. This deviation also provides smaller MFD and thus slightly larger nonlinearity at 800 nm, as Fig. 6(b) shows. The combined action of small normal dispersion and stronger nonlinearity provides excessive spectral broadening and development of a strong 10.9 dB dip in the central part of the spectrum for ($\Lambda, d + 10\%$), as Fig. 6(d) shows. This spectral distortion is accompanied by weak distortion of the pulse envelope in the temporal domain at the top of the pulse shown in the Fig. 6(c). It is related to the small amount of normal dispersion, when the dispersion curve is close to zero at the pump wavelength. Further reduction of the normal dispersion and transition to the anomalous dispersion regime leads to the splitting of the pulse and actually destroys the single pulse propagation [18]. In this case, we obtain SC spectra with two ZDWs [8-10]. If we take a smaller deviation ($\Lambda, d + 5\%$), this dip in the spectral part of the spectrum is smaller than 4.4 dB. In the opposite case, when the air hole's diameter is reduced ($\Lambda, d - 5\%$; $\Lambda, d - 10\%$), we obtain shorter SC spectra. Due to the larger normal dispersion and smaller nonlinearity, the spectral broadening is weak, meaning that spectral width is smaller and a larger amount of energy is located in the central part of the spectrum, as Fig. 6(d) shows.

#224230 - $15.00 USD Received 1 Oct 2014; revised 5 Nov 2014; accepted 11 Nov 2014; published 26 Nov 2014

The appearance of the strong dip in the case ($\Lambda, d+10\%$) also provides poor pulse compression if a quadratic compressor is used (Fig. 6(e)). The duration of the compressed pulse in this case is quite small (8.8 fs). However, the peak power drops by ~40 kW. That is, a considerable portion of the pulse energy transfers to the wide-low intensity pedestal. In the case ($\Lambda, d-10\%$) the compression of the pulse is also worse than the compression of the pulse in the case without fabrication errors. However, in case ($\Lambda, d-10\%$), it is rather related to the smaller spectral width of the spectrum. Fig. 6(f) shows results for full phase compensation. In the case ($\Lambda, d-10\%$) the compression of the pulse is also bad due to the smaller spectral width, whereas in the case ($\Lambda, d+10\%$) we can obtain a compressed pulse with a slightly smaller duration and a larger peak power due to the wider spectrum. However, one has to note that the low-intensity oscillating tails in this case are stronger due to the complex spectral shape of the pulse.

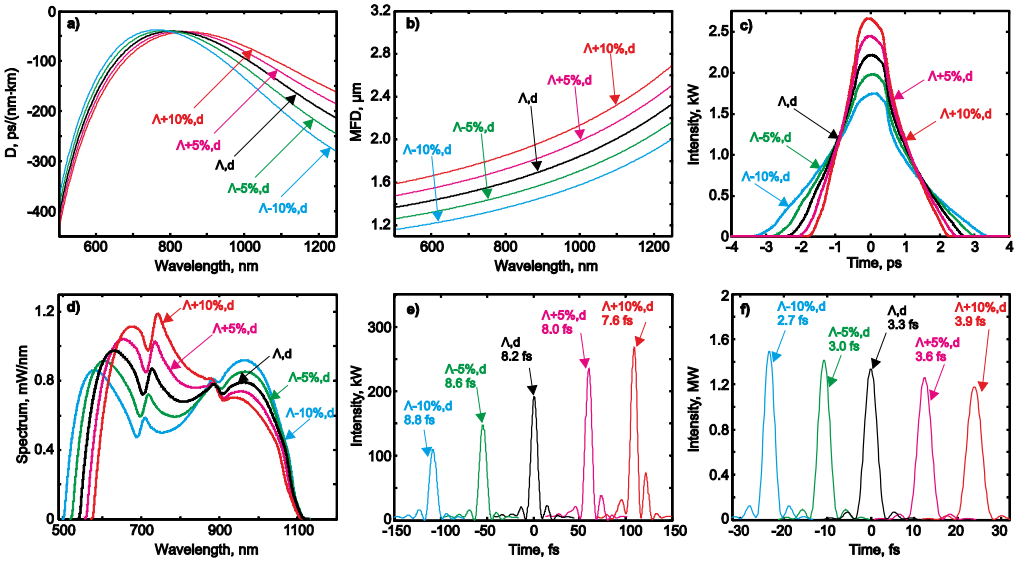

Fig. 7. The influence of fabrication errors on the properties of all-normal dispersion photonic crystal fiber (ANDi PCF), supercontinuum (SC) spectrum, and pulse compression. Only pitch is changed ($\Lambda \pm 5\%, d$; $\Lambda \pm 10\%, d$). a) Fiber's dispersion. b) Mode field diameter (MFD). c) Pulse profiles in temporal domain. d) Pulse spectra. e) Compressed pulses with compensation of only a linear chirp. f) Compressed pulses, full phase compensation.

For a given pump pulse an acceptable compromise between spectral flatness and bandwidth is achieved when nonlinearity is balanced by the proper amount of normal dispersion. This is the case when the SC is generated in ANDi PCFs with the exact design parameters. Nevertheless, we could conclude that $\Lambda, d \pm 3\%$ is the acceptable deviation because within this range the spectral broadening is still large and the central dip is smaller than 4.4 dB. Within this range, one can also achieve stable pulse compression using both quadratic pulse compression (compressed pulse duration < 9.2 fs) and full phase compensation (compressed pulse duration < 3.8 fs).

Next, we investigated the effects of a deviation of the pitch from the designed value. Fig. 7(a) shows the dispersion curves of ANDi PCFs in this case. The main feature in this case is the spectral shifting of dispersion curve maxima, such that pumping wavelength does not coincide with the top of the dispersion curve. When the pitch is increased by 10 % **(** $\Lambda+10\%, d$ **)** the top of the dispersion curve is redshifted to ~850 nm. In this case, the MFD becomes larger (nonlinearity weaker) at 800 nm, as Fig. 7(b) shows. Redshifting of the dispersion curve and weaker nonlinearity give rise to the formation of an asymmetrical

#224230 - $15.00 USD Received 1 Oct 2014; revised 5 Nov 2014; accepted 11 Nov 2014; published 26 Nov 2014

spectrum with reduced spectral width, shown in Fig. 7(d). In this case, the shorter wavelength part of the SC spectrum is strongly raised, whereas the longer wavelength part is reduced. The drop of spectral intensity in the central part of the spectrum is 2.4 dB. When the pitch is maximally decreased **(** $\Lambda - 10\%, d$ **)** the top of the dispersion curve is blueshifted to 750 nm and nonlinearity is larger in this case. This provides for the formation of the spectrum with the largest spectral width, as shown in Fig. 7(d). The spectral shape is nearly symmetrical in this case, and the longer wavelength part of the spectrum is only slightly higher than the shorter wavelength part. However, a dip in the central part of the spectrum is developed (2.8 dB). The compression of the pulse in this case by quadratic compressor is the worst, as Fig. 7(e) shows. Contrary to that, for the case ($\Lambda + 10\%, d$) we obtain the maximal peak power (up to 260 kW) and the shortest pulse duration (7.6 fs). This is achieved in spite of smaller spectral width in this case. This can be explained by the smaller nonlinear coefficient of the fiber in this case, which makes the uncompressed nonlinear chirp smaller. If full phase compensation is applied, then shorter pulses are obtained for larger spectral bandwidth and vice versa, as Fig. 7(f) shows.

Therefore, we can conclude that the positive deviation of pitch is acceptable up to $\Lambda + 5\%, d$ because a larger deviation leads to considerable asymmetry of the spectrum and a reduction of the spectral bandwidth. The negative deviation of pitch is acceptable up to nearly $\Lambda - 7\%, d$ because even in this case the spectrum is quite symmetrical and the dip at the central part of the spectrum is not too considerable (< 2.8 dB). Within this range, one can also achieve a stable pulse compression using both quadratic pulse compression (compressed pulse duration 8.0-8.6 fs) and full phase compensation (compressed pulse duration 3.0-3.6 fs).

During the fabrication process, the deviations of the pitch and diameter of air holes can also arise simultaneously. We also investigated this case. Fig. 8 shows the fiber's properties and SC spectra when the pitch and hole diameter are increased or decreased simultaneously. From Fig. 8(a) we can see that the dispersion curve is rising and its top is shifted to the longer wavelengths when both d and Λ are increased. For the maximal positive deviation ($\Lambda + 10\%$, $d + 10\%$) the top of the dispersion curve is already close to zero at 850 nm. This leads to the maximal spectral broadening of the corresponding SC spectrum (Fig. 8(d), although the spectral shape is highly asymmetrical with a dip of 6.9 dB in the central part. This happened despite the slightly larger MFD (smaller nonlinearity), as shown in Fig. 8(b). Smaller positive deviation ($\Lambda + 5\%$, $d + 5\%$) leads to a dip of 3.8 dB in the central part of the spectrum. The maximal negative deviation ($\Lambda - 10\%$, $d - 10\%$) shifts the dispersion curve downward and moves its top to 750 nm, as Fig. 8(a) shows. This leads to minimal spectral broadening of the corresponding SC spectrum in Fig. 8(d) with a high intensity top in the central part. From Fig. 8(e) one can see that the best compression is achieved for the case without fabrication errors if a quadratic compressor is used. Even for smaller deviations ($\Lambda \pm 5\%$, $d \pm 5\%$) the peak power of the compressed pulse is reduced to 110 kW and the pulse duration rises to 9-9.5 fs. If a full phase compensation is applied, then shorter pulses are obtained for larger spectral bandwidth and vice versa, as Fig. 8(f) shows. However, the changes in compressed pulse peak power and duration are quite small.

Thus we can conclude that the simultaneous and positive deviation of pitch and hole diameter is acceptable up to ($\Lambda \pm 3\%$, $d \pm 3\%$) because larger deviation leads to the strong asymmetry of the spectrum and development of the strong dip in the central part of the spectrum or vice versa to the insufficient spectral broadening. Within this range the central dip has to be smaller (3.8 dB) and one can also achieve stable pulse compression using both quadratic pulse compression (compressed pulse duration < 9.5 fs) and full phase compensation (compressed pulse duration < 3.5 fs).

#224230 - $15.00 USD Received 1 Oct 2014; revised 5 Nov 2014; accepted 11 Nov 2014; published 26 Nov 2014

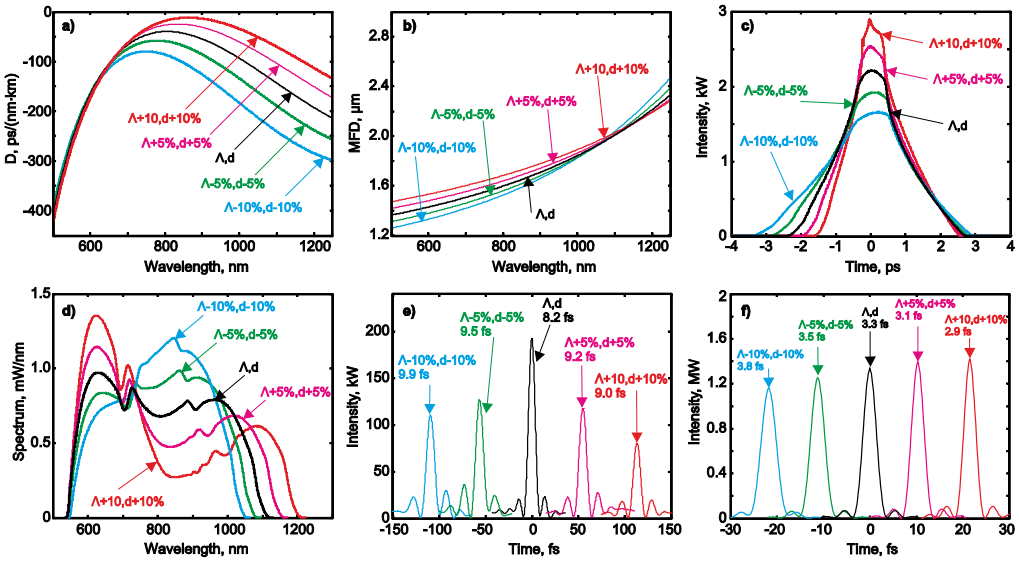

Fig. 8. The influence of fabrication errors on the properties of all-normal dispersion photonic crystal fiber (ANDi PCF), supercontinuum (SC) spectrum, and pulse compression. Both diameter of air holes and pitch are changed ($\Lambda \pm 5\%$, $d \pm 5\%$; $d \pm 10\%$, $\Lambda \pm 10\%$). a) Fiber dispersion. b) Mode field diameter (MFD). c) Pulse profiles in temporal domain. d) Pulse spectra, e) Compressed pulses with compensation of only a linear chirp. f) Compressed pulses, full phase compensation.

Fig. 9 shows the fiber's properties, the SC spectra, and pulse compression when the pitch and hole diameter are increased or decreased in the opposite manner. From Fig. 9(a) we can see that the top of the dispersion curve rises and shifts slightly to shorter wavelengths when Λ is decreased and d is increased. For the case ($\Lambda - 10\%$, $d + 10\%$) the top of the dispersion curve is very close to zero and nonlinearity is larger due to the smaller MFD at 800 nm, as Fig 9(b) shows. Owing to that, the corresponding spectrum at Fig. 9(d) is highly broadened and its central part is depleted nearly down to zero (a dip of 19.1 dB). In this case, one can also see the appearance of pulse temporal envelope distortions, as Fig. 9(c) shows. Smaller deviation ($\Lambda - 5\%$, $d + 5\%$) leads to a dip of 5.2 dB in the central part of the spectrum. For the opposite case ($\Lambda + 10\%$, $d - 10\%$) the dispersion curve falls down and nonlinearity becomes smaller, leading to very weak spectral broadening, as shown in Fig. 9(d). From Fig. 9(e) we can see that the development of such a strong dip in the case ($\Lambda - 10\%$, $d + 10\%$) leads to poor compression if a quadratic compressor is used. The peak power of the compressed pulse drops to 13 kW due to the fact that most of the pulse energy transfers to the low-intensity wings. In the case of opposite deviation ($\Lambda + 10\%$, $d - 10\%$) the result of pulse compression is better. The peak power of the compressed pulse is even somewhat larger compared to the case without fabrication errors; however the duration of the pulse is also larger and the oscillated tail is quite considerable. From Fig. 9(f) we can see that the strong spectral broadening in the case ($\Lambda - 10\%$, $d + 10\%$) provides a very short compressed pulse with a duration of 2.0 fs if full phase compensation is applied. However, one has to note also that in this case the oscillated low-intensity tails are quite considerable due to the complex spectral shape of the pulse.

On the basis of these results, we can conclude that opposing deviations of pitch and hole diameter are acceptable up to ($\Lambda \mp 3\%$, $d \pm 3\%$) because larger deviation leads to either strong depletion of the central part of the spectrum or insufficient spectral broadening. Within this range the central dip has to be smaller than 5.2 dB, and one can also achieve stable pulse

#224230 - $15.00 USD Received 1 Oct 2014; revised 5 Nov 2014; accepted 11 Nov 2014; published 26 Nov 2014

compression using both quadratic pulse compression (compressed pulse duration < 8.8 fs) and full phase compensation (compressed pulse duration < 4.1 fs).

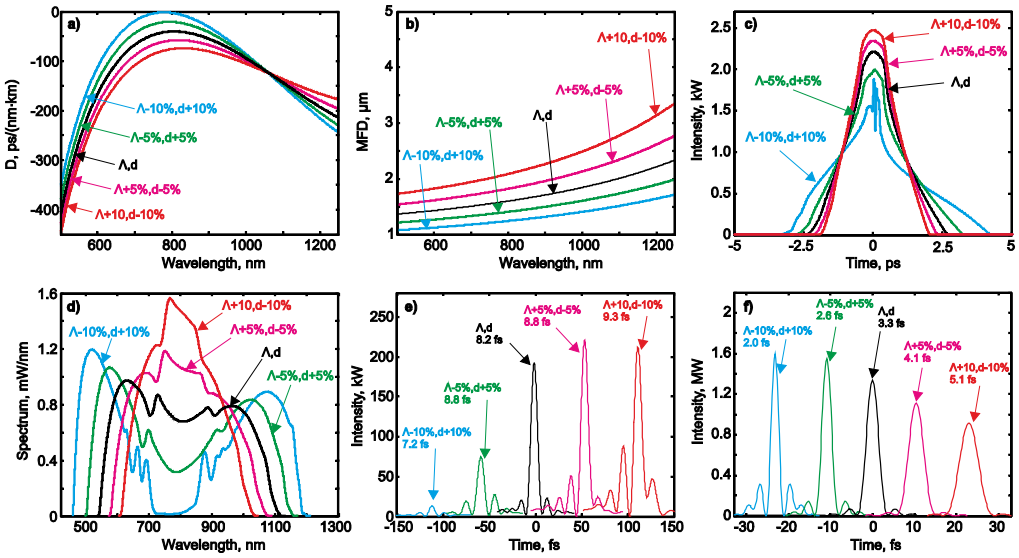

Fig. 9. The influence of fabrication errors on the properties of all-normal dispersion photonic crystal fiber (ANDi PCF), supercontinuum (SC) spectrum and pulse compression. Both diameter of air holes and pitch are changed ($\Lambda \pm 5\%$, $d \mp 5\%$; $\Lambda \pm 10\%$, $d \mp 10\%$). a) Fiber dispersion. b) Mode field diameter (MFD). c) Pulse profiles in temporal domain. d) Pulse spectra. e) Compressed pulses with compensation of only a linear chirp. f) Compressed pulses, full phase compensation.

We can see that different deviations of the fiber's design parameters lead to various changes in the SC spectra. In some cases these spectral changes are unacceptable due to the strong depletion of the central part, strong spectral asymmetry, or insufficient spectral broadening. For example, the separate deviation of the pitch is acceptable up to 5-7%. However, the deviation of the diameter of air holes leads to the stronger spectral distortions. Thus, in general one can conclude that the deviations of either diameter of air holes or pitch are fully acceptable up to 3%.

7. Correction the negative impact of the fabrication errors by variation of pump

From Section 6 one can conclude that fabrication errors (5-10%) could significantly influence the SC generation in ANDi PCFs and pulse compression. The most important factor is the shifting of the peak of the dispersion curve relative to the pump wavelength. Rising or falling of the dispersion curve (vertical shifting) leads to the decreasing of spectral width or excessive spectral broadening, such that the dip in the central part of the spectrum appears. The shifting of the dispersion curve over the spectral axes (horizontal shifting) leads to the asymmetrical spectral broadening. In other cases, some combination of these distortions takes place. The changing in the nonlinear coefficient due to the fabrication errors (5-10%) slightly influences the spectral shape. On the other hand, from Sections 4 and 5 one can see that variation of the pump pulse parameters provides similar changes in the spectral shape. In particular, the changing of peak power of the pump pulse allows for the strength of spectral broadening to be tuned, whereas the shifting of the pump pulse wavelength allows the mismatch between the pump wavelength and peak of dispersion curve to be compensated for. Thus, we can assume that the proper variation of the pump would permit the negative impact of the fabrication errors on the spectral shape of the SC in ANDi PCF to be precisely corrected. In this section, we verify this hypothesis.

#224230 - $15.00 USD Received 1 Oct 2014; revised 5 Nov 2014; accepted 11 Nov 2014; published 26 Nov 2014

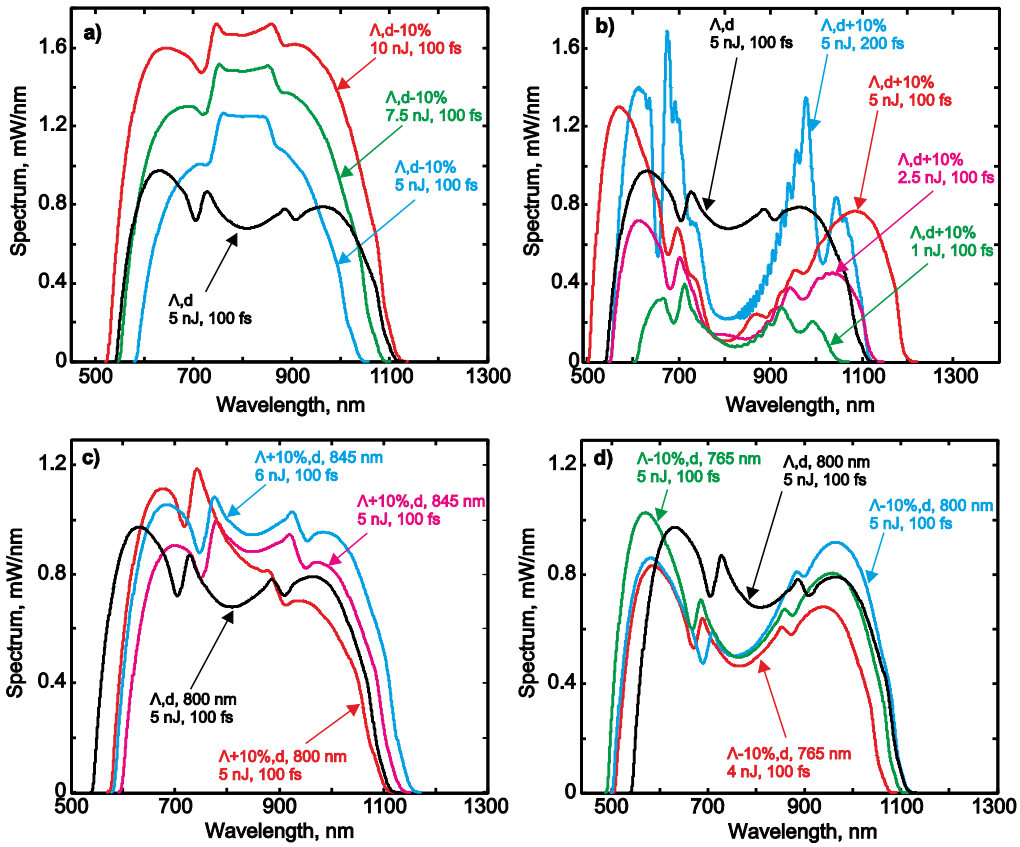

Fig. 10. Correction of spectral shape by tuning the pump. a) Correction of spectral shape for the case of fabrication error $d\Lambda$ – , 10% (see Fig. 6). b) Correction of spectral shape for the case of fabrication error $d\Lambda$ + , 10% (see Fig. 6). c) Correction of spectral shape for the case of fabrication error $\Lambda + 10\%$, d (see Fig. 7). d) Correction of spectral shape for the case of fabrication error $\Lambda - 10\%$, d (see Fig. 7). Peak powers of pump pulses are (color coded) 44 kW, 52.8 kW, 44 kW, 44 kW, 44 kW.

Fig. 10 shows the results of correcting the spectral shape by manipulating the pump for some cases of fabrication errors. Fig. 10(a) shows the results of correcting for insufficient spectral broadening (the case $\Lambda, d-10\%$; 5 nJ, 100 fs) by changing the pump peak power. The reason of this insufficient spectral broadening is shift down of the dispersion curve as Fig. (6a) shows. In order to compensate for this we increase the peak power of the pump. Fig. 10(a) shows that increasing the pulse energy easily allows for the spectral width of the SC to be increased. In particular, for the case (10 nJ, 100 fs; peak power 94 kW) the spectral width already exceeds the spectral width of SC spectra for the original design of the ANDi PCF without fabrication errors and optimal pump (Λ, d; 5 nJ, 100 fs). Moreover, the spectral flatness here is perfect even for increased pulse energy up to 10 nJ. In other words, the drop of spectral intensity at the central part of the spectrum here is about 0.7 dB. Thus, in this case one can achieve an efficient correction of the insufficient spectral broadening.

Fig. 10(b) shows the results of correction of excessive spectral broadening with a strong dip (10.9 dB) in the spectrum for the case ($\Lambda, d+10\%$; 5 nJ, 100 fs) by changing the pump peak power. The reason for this excessive spectral broadening is the rise in the top of the dispersion curve (smaller normal dispersion) as Fig. 6(a) shows. In order to compensate for this we decrease the peak power of the pump. However, from Fig. 10(b) we can see that the

#224230 - $15.00 USD Received 1 Oct 2014; revised 5 Nov 2014; accepted 11 Nov 2014; published 26 Nov 2014

reduction of the pulse energy, even up to 1 nJ (for 100 fs; peak power 9.4 kW), does not provide sufficient attenuation of the dip in the central part. The drop in spectral intensity at the central part of the spectrum is still large (7 dB), whereas the spectral width is reduced considerably in this case due to the smaller pump pulse energy. We conclude that this is the wrong way to eliminate the spectral dip. The increasing of the pulse width up to 200 fs, 5 nJ (peak power 23.5 kW) also does not lead to the elimination the spectral dip, as Fig. 10(b) shows. Therefore, we conclude that the variation of the pump is ineffective if a strong dip in the spectrum is present due to fabrication errors.

Fig. 10(c) shows the results of correcting the spectral shape asymmetry (the case of $\Lambda+10\%, d$; 5 nJ, 100 fs) by shifting the pump wavelength and changing the pump peak power. The reason for this spectral asymmetry is the redshift of the top of the dispersion curve up to 845 nm (see Fig. 7(a)). Thus, in order to compensate for this we shift the pump wavelength to 845 nm as well. This effectively eliminates the asymmetry of the spectrum, as Fig. 10(c) shows. However, the spectral width is smaller in this case as compared to the SC spectra for the original design of ANDi PCF without fabrication errors and the optimal pump at 800 nm (Λ, d ; 5 nJ, 100 fs). This can be explained by the fact that the nonlinear coefficient of the fiber is smaller at longer wavelengths. Therefore, it is reasonable to also increase the peak power pump in this case. From Fig. 10(c) one can see that for the pump 6 nJ, 100 fs (peak power 56.4 kW) the spectral width increases and the spectral flatness is sufficient (a drop of only 0.9 dB).

Fig. 10(c) shows the results of correcting the spectral shape asymmetry (the case of $\Lambda-10\%, d$; 5 nJ, 100 fs) by shifting the pump wavelength and changing the pump peak power. The reason for this spectral asymmetry is the blueshift of the top of the dispersion curve up to 765 nm (see Fig. 7(a)). In this case, the spectral asymmetry is not too significant; therefore shifting the pump to the top of dispersion curve at 765 nm does not lead to sufficient improvement of the pulse shape, as Fig. 10(c) shows. However, if we reduce the pump pulse energy from 5 to 4 nJ, this allows the spectral dip to slightly decrease from 3.2 dB to 2.5 dB, whereas the spectral width will be the same as those in the case of the original design of the ANDi PCF without fabrication errors and an optimal pump at 800 nm (Λ, d ; 5 nJ, 100 fs).

One can see that by varying the pump power parameters – i.e., peak power and wavelength – one is able to sufficiently correct most of the spectral shape distortions due to the fabrication errors (up to 10%).

8. Conclusions

We have designed an ANDi PCF with a flat-top dispersion curve at 800 nm. The SC generated by applying conventional Ti:Sapphire laser pulses was numerically investigated. The impact of pump pulse parameters, such as pump pulse energy and pulse duration, on the generated SC and compression of pulses was also investigated. The optimal combination of pump pulse parameters was found to be a pulse energy of 5 nJ, along with a pulse duration of 100 fs, which provides maximal spectral width (~ 1 octave) and perfect spectral flatness (a drop of ~1.7 dB in spectral intensity). The compression of pulses with such spectra allows multiple-cycle pulses (~8 fs) to be obtained if a simple quadratic compressor is used, and allows single-cycle pulses (3.3 fs) to be obtained if full phase compensation is applied. The impact of pump pulse wavelength shifting with respect to the top of dispersion curve on the generated SC and pulse compression was also investigated. The optimal pump pulse wavelength range was found to be $750\,\text{nm} < \lambda_p < 850\,\text{nm}$, which is around the design wavelength of 800 nm, where the distortions of pulse shape are quite small (< 3.3 dB dip) and pulse compression provides comparable results with those generated when the pump is at exactly 800 nm. Conversely, larger deviation of the pump pulse wavelength from the top of dispersion curve leads to strongly asymmetrical spectral distortions and worsened compression results.

#224230 - $15.00 USD Received 1 Oct 2014; revised 5 Nov 2014; accepted 11 Nov 2014; published 26 Nov 2014

The influence of realistic fiber fabrication errors on the SC generation and pulse compression were investigated systematically. The errors in the diameters of air holes lead to the rising or falling of the fiber's dispersion curve, which further leads to either a decrease in spectral width or excessive spectral broadening, such that the dip in the central part of the spectrum appears. On the other hand, the errors in the pitch give rise to preliminary the shift in the fiber's dispersion curve over the spectral axes, leading to asymmetrical spectral broadening. If both errors are present, this leads to some combination of those distortions. It was found that the independent deviation of the pitch is acceptable up to 5-7%. However, the deviation of the diameter of air holes leads to stronger spectral distortions. Thus, in general the deviations of either diameter of air holes or pitch are fully acceptable up to 3%. Nevertheless, we have shown that proper variation of the pump power parameters is able to sufficiently correct most of the spectral shape distortions due to the fabrication errors (up to 10%).

Acknowledgements

This work was supported by University of Guanajuato (projects DAIP-192/13 and DAIP-334/13), by SEP/PROMEP (project UGTO-PTC-371), and in part by the Ministerio de Economía y Competitividad and the Generalitat Valenciana of Spain under projects TEC-2013-46643-C2-1-R and PROMETEO II/2014/072, respectively. Publication of this work is funded by University of Guanajuato through the PIFI program.

#224230 - $15.00 USD Received 1 Oct 2014; revised 5 Nov 2014; accepted 11 Nov 2014; published 26 Nov 2014